ETH zürich

ETH Library

Solvated Electrons in Clusters: Magic Numbers for the Photoelectron Anisotropy

Journal Article

Author(s):
West, Adam H.C.; Yoder, Bruce L.; Luckhaus, David; Signorell, Ruth

Publication date:
2015-09

Permanent link:
https://doi.org/https://doi.org/10.3929/ethz-b-000107184

Rights / license:
In Copyright - Non-Commercial Use Permitted

Originally published in:
The Journal of Physical Chemistry A 119(50), https://doi.org/10.1021/acs.jpca.5b07629

Funding acknowledgement:
- Interaction of Light with Ultrafine Aerosol Particles II ()

This page was generated automatically upon download from the ETH Zurich Research Collection.
For more information, please consult the Terms of use.

Solvated Electrons in Clusters: Magic Numbers for the Photoelectron Anisotropy

*Adam H. C. West, Bruce L. Yoder, David Luckhaus, and Ruth Signorell**

ETH Zürich, Laboratory of Physical Chemistry, Vladimir-Prelog-Weg 2, CH-8093, Zürich, Switzerland

Date: August 8, 2015

Submitted to JPC A

Keywords: photoelectron spectroscopy, anisotropy parameter, Na-doping method

* To whom correspondence should be addressed. E-mail: rsignorell@ethz.ch

ABSTRACT

This paper reports on a curiosity concerning magic numbers in neutral molecular clusters; namely on magic numbers related to the photoelectron anisotropy in angle-resolved photoelectron spectra. With a combination of density functional calculations and experiment, we search for magic numbers in $Na(H_2O)_n$, $Na(NH_3)_n$, $Na(CH_3OH)_n$, and $Na(CH_3OCH_3)_n$ clusters. In clusters of high symmetry, the highest occupied molecular orbital can be delocalized over an extended region forming a symmetric charge distribution of high s-character, which results in a pronounced anisotropy in the photoelectron angular distribution. We find magic numbers at n = 6 and n = 4 for sodium-doped dimethyl ether and ammonia clusters, respectively, but not for sodium-doped water and methanol clusters, which is likely a consequence of the degree of hydrogen bonding and the number of structural isomers.

1. Introduction

Numerous mass spectrometric studies for various types of clusters report on so-called 'magic numbers' related to the cluster stability.[1-4] Magic numbers related to the stability have also been mentioned for molecular clusters that exhibit solvated electrons, such as pure anion clusters ($(H_2O)_n^-$, $(NH_3)_n^-$ etc.) or neutral sodium-doped molecular clusters ($Na(H_2O)_n$, $Na(NH_3)_n$ etc.) (see references in [5-9]_ENREF_5_ENREF_5). In this context the solvated electron refers to an unpaired electron located either at the surface of the cluster or inside the cluster volume. The special properties of the solvated electron - in particular its ability to spatially delocalize - make it an attractive candidate to search for a different type of magic number, namely those related to the photoelectron anisotropy. In particular, for molecular clusters of high symmetry it is conceivable that the character of the solvated electron for such a symmetric cluster can differ strongly from that of its neighboring-size, less symmetric clusters. However, to the best of our knowledge no magic numbers related to the photoelectron anisotropy for solvated electrons in clusters have been reported so far, even though many clusters with high symmetry have been predicted by calculations (see references in [5, 7-12]_ENREF_7). This might be a consequence of the fact that the photoelectron anisotropy has not received broad attention, likely because measurements of the photoelectron angular distribution (PAD) of clusters are rather sparse[5, 13-23]_ENREF_13_ENREF_7_ENREF_7_ENREF_7_ENREF_7_ENREF_7 and because it is difficult to calculate the anisotropy.[15, 17, 24-28] For metallic clusters, by contrast, magic numbers related to the anisotropy have been reported, typically for clusters of high symmetry.[14, 29] In contrast to metallic clusters, molecular clusters are held together by a fine balance of weak intermolecular forces with different distance- and orientation-dependencies (electrostatic, induction, dispersion, hydrogen bonds). Even small contributions of certain intermolecular interactions can thus strongly influence the geometry of the clusters, probably making them less likely to form perfectly symmetric structures. Furthermore, many structural isomers with similar energies can exist for the same cluster size, so that even size-selection (currently only broadly possible for charged clusters) does not help to select a specific structure. Both factors could make the observation of magic numbers less likely compared with metallic clusters.

The present study reports on our search for magic numbers related to the photoelectron anisotropy of the solvated electron in $Na(H_2O)_n$, $Na(NH_3)_n$, $Na(CH_3OH)_n$, and $Na(CH_3OCH_3)_n$ clusters. These neutral clusters exhibit solvated electrons but have the disadvantage of weak intermolecular interactions and, because they are uncharged, the lack of size-separation. In a first step, we use density functional (DFT) calculations to search for clusters of high symmetry and to calculate the β-parameters that describe the PAD of these clusters. In a second step, we compare the modeling results with corresponding experimental data extracted from angle-resolved photoelectron spectra of these clusters. Part of the experimental data has been reported recently in ref. [23]. We conclude the paper with a short discussion of how and when it is likely to observe such magic numbers experimentally.

2. Experiment and calculations

The experimental setup used for this study is described in detail in refs. [20-23, 30-32], so that we only provide a brief description here. The solvent clusters $(H_2O)_n$, $(NH_3)_n$, $(CH_3OH)_n$, and $(CH_3OCH_3)_n$ are formed in free supersonic expansions. The solvent cluster beam traverses a Na-oven where single Na atoms are picked up by the solvent clusters resulting in the Na-doped clusters $Na(H_2O)_n$, $Na(NH_3)_n$, $Na(CH_3OH)_n$, and $Na(CH_3OCH_3)_n$. The Na-doped clusters then enter the ionization/detection chamber, where they are ionized with a 266 nm

Nd:YAG laser. This photon energy (4.66 eV) is chosen in order to ionize exclusively the solvated (unpaired) electron. The ionization/detection chamber is used to record time-of-flight (TOF) mass spectra of the Na-doped clusters as well as angle-resolved photoelectron spectra. The mass spectra provide information on the cluster size distribution that is probed by photoelectron spectroscopy. Note that size-selection before recording the photoelectron spectra is not possible for uncharged Na-doped clusters. An independent measurement of the cluster size-distribution (here using mass spectrometry[20, 23]) is therefore crucial. Furthermore, the relative intensities in the mass spectra can provide information on the relative stability of different cluster sizes (i.e. on magic numbers related to cluster stability). The photoelectron spectra of the clusters are recorded with a velocity map imaging setup.[33, 34] The corresponding photoelectron images contain information on the kinetic energy of the photoelectrons and their angular distribution. Ionization energies (IEs) are extracted from the electron kinetic energies and the photon energy used for ionization. The experimental IEs, denoted IE_{max}, are determined at the maximum of the photoelectron band. It is assumed that these values lie close to the vertical IEs. The PAD,

$$\frac{d\sigma}{d\Omega} = \frac{\sigma_{tot}}{4\pi}\left[1 + \frac{\beta}{2}\left(3\cos^2\theta - 1\right)\right], \qquad \text{Eq. (1)}$$

is characterized by the anisotropy parameter β,[35] where $\frac{d\sigma}{d\Omega}$ and σ_{tot} are the differential and the total photoionization cross section, respectively, and θ is the angle between the photoelectron velocity vector and the polarization axis of the incident light. We estimate the absolute uncertainties in IE_{max} and β to be on the order of ± 0.1 eV and ± 0.1, respectively. However, relative errors for a series of clusters of different size are presumably smaller. From the statistics of independent measurements we estimate the uncertainty of the *change* of IE_{max} and β with cluster size to be ~ 5 % in both cases.

Optimized structures of Na-doped neutral and Na-doped ionic clusters are calculated with the Gaussian program package[36] using the dispersion corrected ωB97XD density functional with a 6-31+G* basis set. We use the enthalpy of vaporization H_{vap} to compare cluster stabilities for different cluster sizes. In this work, H_{vap} is calculated for the neutral clusters as the total dissociation energy divided by the number of solvent monomer units. In section 3, we also indicate the total dipole moments of the different neutral clusters as a simple measure of the charge distribution. Vertical ionization energies (IE_{vert}) are determined by subtracting the energy of the neutral cluster from the energy of the ionic cluster with the same geometry. For the calculations of the β-parameters, the highest occupied molecular orbital (HOMO) is expanded in terms of atomic natural orbitals (ANOs).[37] The normalized angular momentum (ℓ) character c_ℓ^2 of the HOMO is calculated as the sum over ANO contributions of the same ℓ. The β-parameters are then obtained from,[16]

$$\beta = \sum_\ell c_\ell^2 \beta_\ell \qquad \text{Eq. (2)}$$

with β_ℓ determined from the Cooper–Zare formula,[35]

$$\beta_\ell = \frac{\ell(\ell-1)(1-R)^2 + (\ell+1)(\ell+2)R^2 - 6\ell(\ell+1)(1-R)R}{(2\ell+1)\left[\ell(1-R)^2 + (\ell+1)R^2\right]} \qquad \text{Eq. (3)}$$

neglecting the phase shift between outgoing partial waves. R is the relative radial dipole matrix element of the (ℓ+1) partial wave. In the present paper, we provide the results for R = 0.5 and for radial matrix elements vanishing at all centers except the Na atom. We have previously shown that the size-dependence of β (not the absolute values) is almost independent of the choice of the parameters (other limiting cases for R and for radial matrix elements for all atomic centers) for Na-doped clusters.[23] This robustness with respect to the parameters and the fact that the simple approach in Eq. 2 and 3 provides suitable results is a consequence of the special properties of the unpaired electron in Na-doped clusters. In these systems, the unpaired electron largely retains the character of a Na valence electron. We refer the reader to ref. [23] and its supporting information for more details. An important point for the present work is that trends in the size-dependence of calculated and experimental β-parameters can be compared, even though their absolute values cannot.

3. Results and Discussion

We use DFT calculations to calculate cluster structures and β-parameters for clusters with up to 18 solvent molecules and search for clusters of high symmetry that have β-parameters that clearly differ from the ones of neighboring cluster sizes. The clearest results are obtained for $Na(CH_3OCH_3)_n$ clusters, for which we find two clusters, $Na(CH_3OCH_3)_6$ and $Na(CH_3OCH_3)_{10}$, with symmetric, delocalized highest occupied molecular orbitals (HOMOs) as depicted in Figs. 1b and d, respectively. The calculated β-parameters provided in Fig. 2a are indeed much higher for these two clusters compared with neighboring cluster sizes and other structural isomers (i.e. for n = 10, shown as the full circle in Fig. 2). The β-values for n = 5 and 7, for example, are significantly lower and the HOMOs of these two clusters do not have a high symmetry but are rather localized on one side of the cluster (see Figs. 1a and c). The high symmetry of the HOMO for n = 6 and 10 is a consequence of the high symmetries of these clusters (almost T_h with octahedral coordination of Na for n = 6, and with four additional monomers on opposing edges of the slightly distorted O_6-octahedron retaining the inversion symmetry for n = 10), which cause the electron to delocalize over an almost spherical shell around the cluster. As a consequence, these electrons have a very high s-character (100% in the calculation) which results in a high β-value. The high cluster symmetry is also reflected in the total dipole moments given in Fig. 2d. While all other cluster sizes (isomer for n = 10) have dipole moments of many Debye, the dipole moment of $Na(CH_3OCH_3)_6$ almost vanishes (0.02 D) and that of the symmetric isomer of $Na(CH_3OCH_3)_{10}$ is comparatively small (0.74 D). However, there is one important difference between the symmetric n = 6 and the symmetric n = 10 cluster. The n = 6 cluster in Fig. 1b is the only structural isomer we can find for this cluster size and, as shown in Fig. 2b, it is the most stable cluster compared with all other cluster sizes (highest H_{vap}). The n = 10 cluster in Fig. 1d, by contrast, is not particularly stable (Fig. 2b) and it is not even the most stable structural isomer with 10 solvent molecules. The most stable n = 10 cluster is about 24 meV more stable (in terms of H_{vap}) (Fig. 2b). This low-energy structural isomer has neither a high symmetry (structure not shown) nor a high β-parameter (Fig. 2a). For clarity we only show the data for the lowest energy isomer for other cluster sizes in Fig. 2 because we only find very few isomers for dimethyl ether clusters and none of them exhibits any special properties compared with the data in Fig. 2.

The highest probability to observe magic numbers related to the photoelectron anisotropy in the experiment is expected for $Na(CH_3OCH_3)_6$, because the calculations predict a high stability of this cluster and essentially no structural isomers with different properties that could obscure the jump in the β-parameter at this size (Fig. 2a). From an experimental point of view, it is also much more likely to observe a jump of β at n = 6 than at n = 10, because up to n = 6 individual size-resolved photoelectron spectra can be recorded while for n > 6 the photoelectron spectra overlap with one another. An example photoelectron image is shown in Fig. 3a together with the corresponding photoelectron spectrum in Fig. 3b. Individual photoelectron signals are visible for n = 5 and 6 (data for n < 5 are not shown in this spectrum), from which size-dependent β-parameters can be extracted. Above n = 6, the IEs of the different cluster sizes lie too close (Fig. 2c) to resolve individual bands for different cluster sizes (see for example figure 1b in ref. [23]). For these sizes only information on the

β-parameters that are averaged over several cluster sizes can be extracted and magic number effects might thus become obscured. This is the case for the experimental data at n = 9, 11 and 18 in Figs. 2e and 2g. Here the ionization energies and β-parameters can only be assigned to the average cluster size contributing to the band in the photoelectron spectrum, determined from the corresponding mass spectra. The anisotropy in the photoelectron image in Fig. 3a already implies a high β-value for n = 6. The experimental β-values as a function of cluster size in Fig. 2e indeed show a jump at n = 6 consistent with the predictions from the simulation in Fig. 2a. $Na(CH_3OCH_3)_6$ is clearly therefore a magic number cluster for the photoelectron anisotropy. Furthermore, according to the calculations (Fig. 2b) it should also be a magic number related to the stability. The mass spectrum in Fig. 2f indeed shows an increase in the peak intensity at n = 6 consistent with the increase in the vaporization enthalpy at this size. The calculated and experimental evolution of the IEs with size agrees almost perfectly (Figs. 2c and g). At ~ n = 6 the decrease in IEs with increasing size starts to level off, indicating the closure of the first solvation shell. As expected, n = 10 cannot be confirmed as a magic number from the experiment (Fig. 2e) because of the lack of size resolution in the photoelectron image and probably also because more stable structural isomers exist for this cluster size.

According to the calculations, Na-doped dimethyl ether clusters are the most promising candidates for observing magic numbers for the anisotropy. The second-best candidates are Na-doped ammonia clusters. In contrast to the dimethyl ether clusters, they have more structural isomers for a given cluster size and the differences in the β-values for asymmetric and symmetric structures are less pronounced (Figs. 4a and 2a). The line in Fig. 4a again shows the β-parameters of $Na(NH_3)_n$ clusters as a function of size for the most stable isomers. The corresponding values for other isomers typically deviate by less than ± 0.2 from these values (data not shown). The HOMOs of these asymmetric clusters are located on one side of the cluster, similar to the situation exemplified by the cluster structure of $Na(CH_3OCH_3)_5$ in Fig. 1a. As for dimethyl ether clusters, this asymmetric charge distribution results in substantial dipole moments (see Fig. 4d). For n = 4, the values of two additional isomers (IA and IC) are provided in Fig. 4 in addition to that of the most stable isomer (IB), the structures of which are shown in Fig. 5. The calculated β-values vary substantially among these isomers (between + 1.34 for IC and + 2.00 for IA). The HOMO of the least stable isomer IC is again located on one side of the cluster (as depicted in Fig. 5c). The vaporization enthalpy of IC lies ~ 60 meV below that of the two almost isoenergetic isomers IA and IB which are therefore expected to dominate in the molecular beam. The tetrahedral arrangement of IA is the only perfectly symmetric structure we find for ammonia clusters of different size. Like the perfectly symmetric $Na(CH_3OCH_3)_6$ cluster, isomer IA has a delocalized and symmetric HOMO (Fig. 5a), with a corresponding β-value of + 2.0, and a vanishing dipole moment (Figs. 4a and d, respectively). There are two versions of this perfectly tetrahedral isomer (symmetry group T_d), one where all the NH_3 units are staggered and one where they are all eclipsed with respect to the Na-N axes. Both have virtually identical properties. Isomer IB represents a class of isomers that differ from IA by slight asymmetries, here the rotation angle of one NH_3 unit around the Na-N axis (i.e. one NH_3 eclipsed, three staggered). There are several such structures with almost identical properties, which are only marginally less stable than isomer IA. In contrast to IA, however, the minor symmetry-breaking causes the HOMO to localize on one side of the cluster (see Fig. 5b), reducing the β-value from + 2.0 to ~ + 1.8 accompanied by a huge increase in the dipole moment from 0 D to more than 5 D. From the energetics it is likely that for n = 4 the molecular beam is dominated by an ensemble of IA-type and IB-type isomers with an average β-value in the range between + 1.8 and + 2.0. Though small, the difference with the β-values of the neighboring cluster sizes n = 3 and n = 5 (β ~ + 1.7 and + 1.5, respectively) might still be observable experimentally. And indeed, the experimental β-values as a function of cluster size in Fig. 4e show a small but clear maximum at n = 4. It is important to note here that for $Na(NH_3)_n$ we can record size-resolved photoelectron spectra and thus size-resolved β-parameters for cluster sizes up to n ~ 4. The photoelectron spectra and β-parameters of larger clusters are always an average over several sizes and over an increasing number of different structural isomers. This might explain why the experimental β-values for n = 5, 6, and 7 decrease only slowly from the maximum at n = 4. While the effect is less pronounced for $Na(NH_3)_4$ than for $Na(CH_3OCH_3)_6$, simulations and experimental results are at least consistent with n = 4 as a magic number for the photoelectron anisotropy of Na-doped ammonia clusters. The mass spectrum in Fig. 4f, however, does not confirm n = 4 as a magic number related to the stability, since no increased ion signal at n = 4 is observed. Finally, similar to Na-doped dimethyl ether clusters, the IEs start to level off between n = 4 and n = 6 (see Figs. 4c and g).

The search for magic numbers in the anisotropy was not successful for $Na(H_2O)_n$ and $Na(CH_3OH)_n$. We believe that hydrogen bonding is the major fundamental reason for this. The directionality of strong hydrogen bonds produces a large number of different isomers in the simulations for each cluster size. Some of them only differ by minor structural changes. These isomers have different β-values so that magic numbers for the anisotropy are less likely to be observable even with size-resolution. With methanol as a solvent, the low symmetry of the monomer further reduces the likelihood of stable highly symmetric structures of which we could find none in the calculations. Consistent with these predictions, we do not observe any magic numbers in the anisotropy (see experimental β-values for methanol in Figure 2 of ref. [23]). For water, by contrast, highly symmetric structures with delocalized symmetric HOMOs are predicted. Fig. 6 shows two examples for n = 6 and n = 12, both with β-values of + 2.0. However, no particularly high values are observed in the experiment (see experimental β-values for water in figure 2 in ref. [23]). The major reason is certainly that the photoelectron spectra of $Na(H_2O)_n$ lack sufficient size resolution above n = 2 because the photoelectron bands in water are very broad and overlap with one another. But even with size-resolution the observation of magic numbers for the anisotropy would be unlikely for Na-doped water clusters because of the many isomers. For n = 6, for example, the calculations predict several isomers with β-values between + 1.0 and + 2.0 and H_{vap} between 302 meV and 467 meV. Furthermore, the perfectly symmetric n = 6 isomer in Fig. 6a lies ~ 1 eV higher in total energy than the most stable isomer, so that its abundance in the cluster beam is presumably insignificant. Strongly hydrogen bonded clusters appear to prefer non-symmetric structures which minimize the perturbation of the H-bond network by 'pushing' the Na atom and its electron to one side of the cluster. This would explain the lower β-values and the absence of magic numbers related to the photoelectron anisotropy.

4. Summary

This paper demonstrates that magic numbers related to the photoelectron anisotropy can be observed in neutral, weakly-bound, molecular clusters. The solvated electron in $Na(H_2O)_n$, $Na(NH_3)_n$, $Na(CH_3OH)_n$, and $Na(CH_3OCH_3)_n$ is chosen for this study because it can delocalize over an extended region and form a symmetric HOMO with high s-character in perfectly symmetric cluster structures. The calculations clearly predict such highly symmetric cluster structures with very high anisotropy parameters β for Na-doped water, ammonia, and dimethyl ether clusters but nor for Na-doped methanol clusters. For water and methanol, the calculations also reveal that many structural isomers exist for a given cluster size that are energetically close, likely due to hydrogen bonding. Most of these isomers do not have a perfectly symmetric structure and thus they also do not have a particularly high value of the β-parameter. It is thus not surprising that magic numbers related to the photoelectron anisotropy cannot be observed experimentally for water and methanol. For dimethyl ether and ammonia, which are less strongly hydrogen bonded, we found magic numbers at n = 6 and n = 4, respectively, as predicted by the calculations. The results of the present study lead us to expect magic numbers for the anisotropy to be a rare experimental observation in the case of molecular clusters. Even if such distinguished clusters exist in the molecular beam it would require isomer-selection in addition to size-selection to be able to observe this phenomenon.

ACKNOWLEDGMENT

We are very grateful to David Stapfer and Markus Steger from our workshop for their help in the realization of the experimental setup. Financial support was provided by the Swiss National Science Foundation under project no. 200020_159205 and by the ETH Zürich.

LIST OF FIGURES

Figure 1. Isosurfaces of the HOMO of a) $Na(CH_3OCH_3)_5$, b) $Na(CH_3OCH_3)_6$, c) $Na(CH_3OCH_3)_7$, and d) $Na(CH_3OCH_3)_{10}$. The calculated s-character of these HOMOs are 55%, 100%, 79%, and 100%, respectively.

Figure 2. Properties of $Na(CH_3OCH_3)_n$ clusters as a function of the number of solvent molecules n: a) calculated β-parameters, b) calculated enthalpies of vaporization H_{vap}, c) calculated vertical ionization energies IE_{vert}, d) calculated dipole moments, e) experimental β-parameters, f) representative mass spectrum, and g) experimental ionization energies determined at the maximum of the photoelectron bands IE_{max}. The open circles connected by lines are the values for the energetically lowest isomers. The full circle for n = 10 is for the highly symmetric $Na(CH_3OCH_3)_{10}$ cluster depicted in Fig. 1d.

Figure 3. a) Experimental photoelectron image of $Na(CH_3OCH_3)_n$ clusters. The raw (before reconstruction) image is shown. b) Corresponding photoelectron spectrum. The broad band below an IE of ~ 1.9 eV contains contributions from all cluster sizes with $6 < n < \sim 25$.

Figure 4. Properties of $Na(NH_3)_n$ clusters as a function of the number of solvent molecules n: a) calculated β-parameters, b) calculated enthalpies of vaporization H_{vap}, c) calculated vertical ionization energies IE_{vert}, d) calculated dipole moments, e) experimental β-parameters, f) representative mass spectrum, and g) experimental ionization energies determined at the maximum of the photoelectron bands IE_{max}. The open circles connected by lines are the values for the energetically lowest isomers. For n = 4 this corresponds to isomer IB (Fig. 5b). The full circle for n =

4 is for the highly symmetric isomer IA depicted in Fig. 5a. The full square is for the asymmetric isomer IC in Fig. 5c.

Figure 5. Isosurfaces of the HOMO of $Na(NH_3)_4$ a) isomer IA b) isomer IB, c) isomer IC. The calculated s-character of these HOMOs is 100%, 93%, and 78%, respectively. For IA the all-eclipsed arrangement of NH_3 is shown. For IB the conformer with one NH_3 eclipsed and three staggered is shown.

Figure 6. Isosurfaces of the HOMO of a) $Na(H_2O)_6$ and b) $Na(H_2O)_{12}$. The calculated s-character of both HOMOs is 100%.

Figure 1.

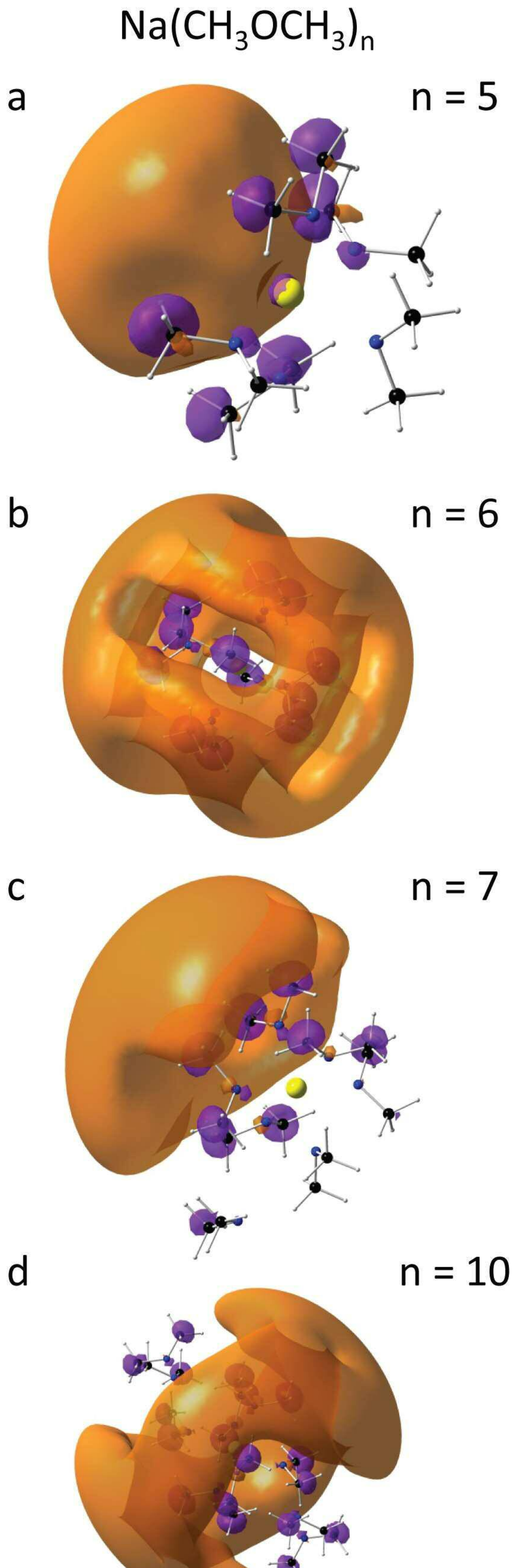

Figure 2.

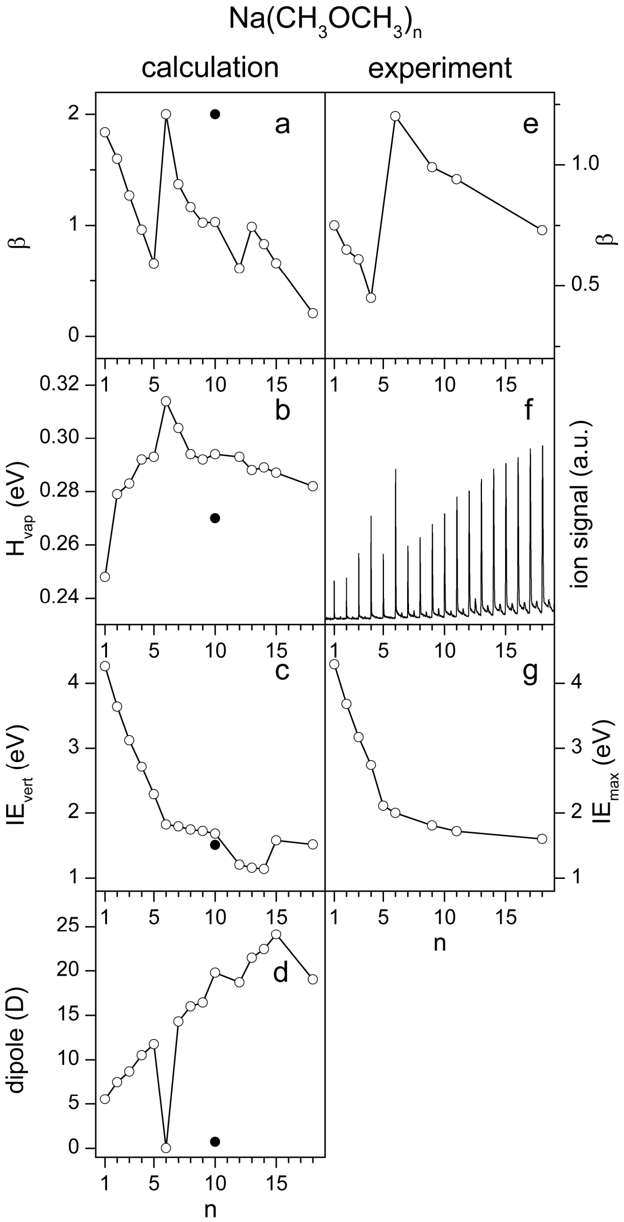

$Na(CH_3OCH_3)_n$
calculation
experiment
a
b
c
d
e
f
g
β
H_{vap} (eV)
IE_{vert} (eV)
dipole (D)
ion signal (a.u.)
IE_{max} (eV)
n

Figure 3.

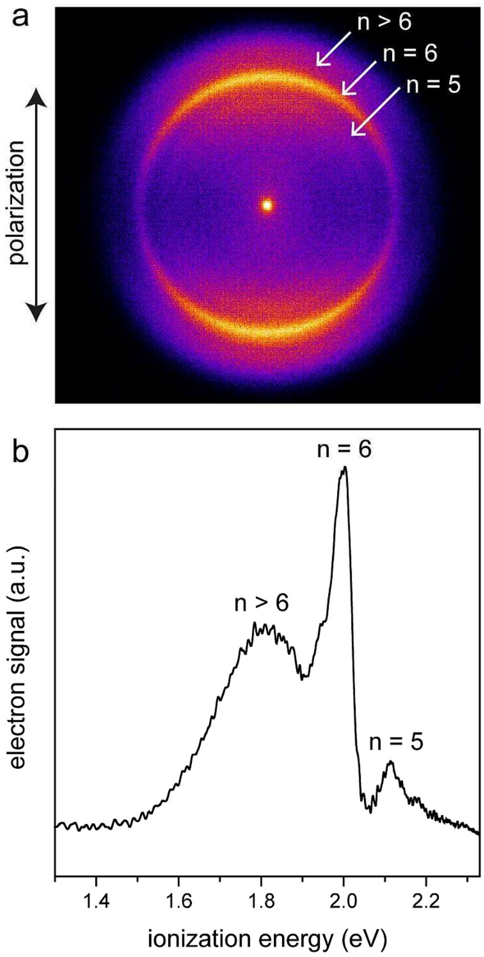
a
n > 6
n = 6
n = 5
polarization
b
n = 6
n > 6
n = 5
electron signal (a.u.)
1.4
1.6
1.8
2.0
2.2
ionization energy (eV)

Figure 4.

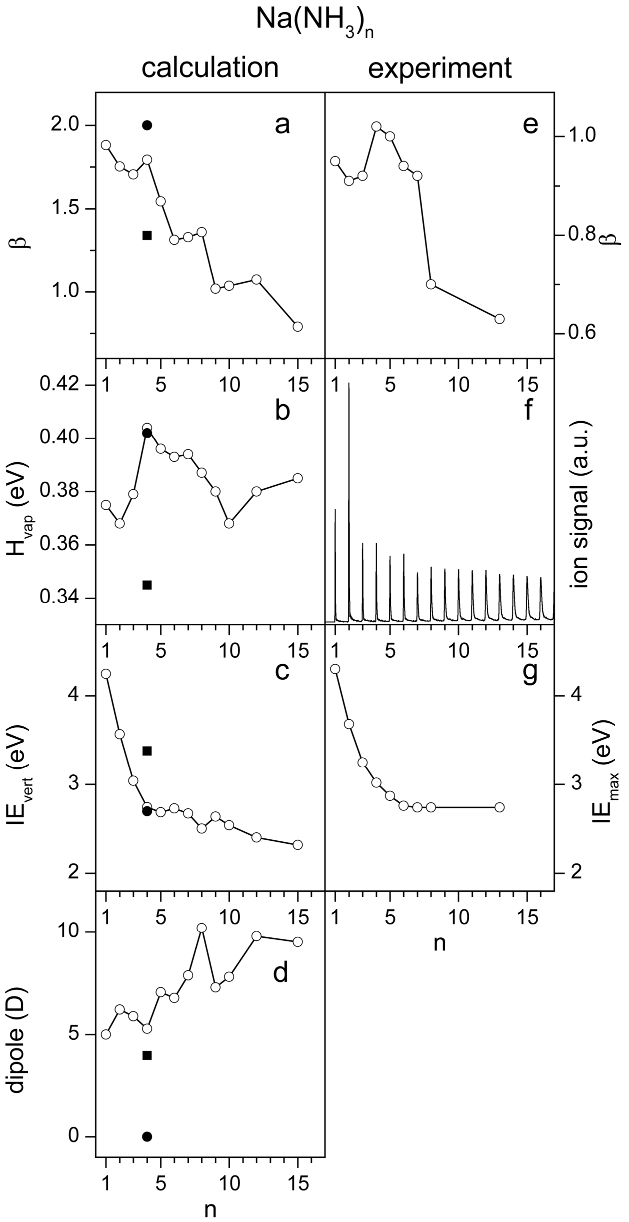
Na(NH$_3$)$_n$
calculation
experiment
a
b
c
d
e
f
g
β
H_{vap} (eV)
IE_{vert} (eV)
dipole (D)
ion signal (a.u.)
IE_{max} (eV)
n

Figure 5.

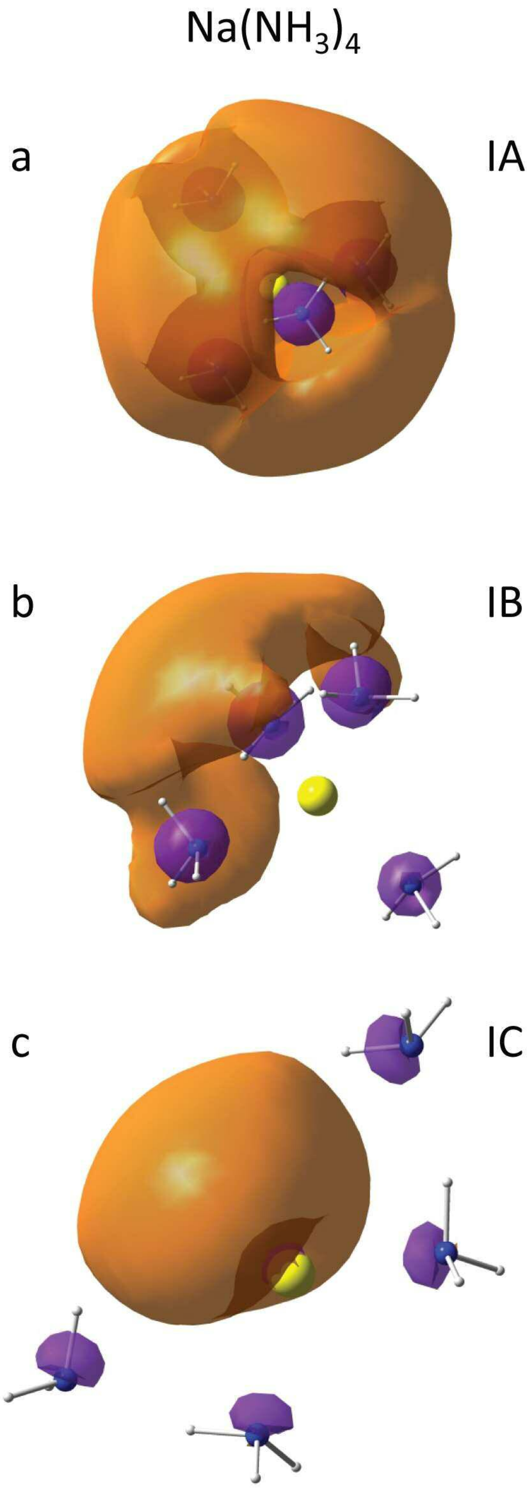

Figure 6.

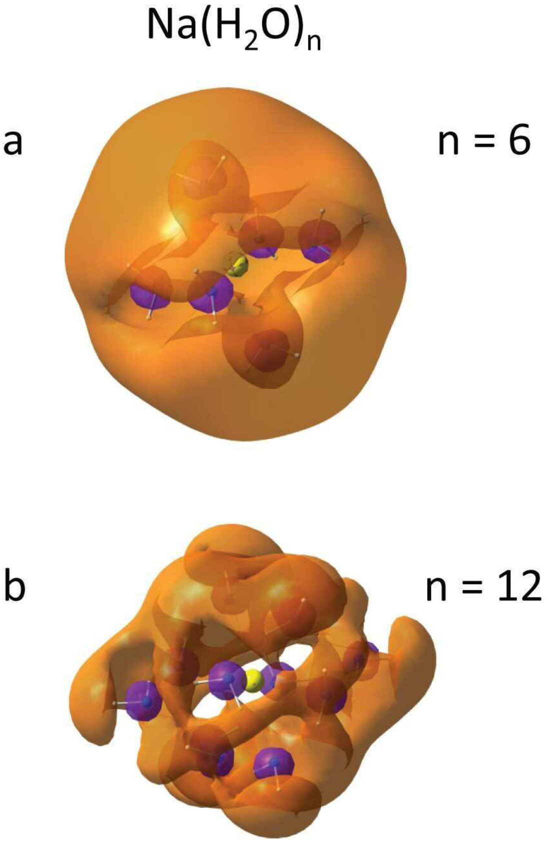

REFERENCES

(1) Vafayi, K.; Esfarjani, K. Abundance of Nanoclusters in a Molecular Beam: The Magic Numbers for Lennard-Jones Potential. *J. Cluster Sci.* **2015**, *26*, 473-490.

(2) Coolbaugh, M. T.; Garvey, J. F. Magic Numbers in Molecular Clusters: A Probe for Chemical-Reactivity. *Chem. Soc. Rev.* **1992**, *21*, 163-169.

(3) Alonso, J. A. Van der Waals Clusters. *Structure and Properties of Atomic Nanoclusters.* **2005**, 21-58.

(4) Chang, H. C.; Wu, C. C.; Kuo, J. L. Recent Advances in Understanding the Structures of Medium-Sized Protonated Water Clusters. *Int. Rev. Phys. Chem.* **2005**, *24*, 553-578.

(5) Young, R. M.; Neumark, D. M. Dynamics of Solvated Electrons in Clusters. *Chem. Rev.* **2012**, *112*, 5553-5577.

(6) Hammer, N. I.; Shin, J. W.; Headrick, J. M.; Diken, E. G.; Roscioli, J. R.; Weddle, G. H.; Johnson, M. A. How Do Small Water Clusters Bind an Excess Electron? *Science.* **2004**, *306*, 675-679.

(7) Turi, L.; Rossky, P. J. Theoretical Studies of Spectroscopy and Dynamics of Hydrated Electrons. *Chem. Rev.* **2012**, *112*, 5641-5674.

(8) Zeuch, T.; Buck, U. Sodium Doped Hydrogen Bonded Clusters: Solvated Electrons and Size Selection. *Chem. Phys. Lett.* **2013**, *579*, 1-10.

(9) Zurek, E.; Edwards, P. P.; Hoffmann, R. A Molecular Perspective on Lithium-Ammonia Solutions. *Angew. Chem.* **2009**, *48*, 8198-8232.

(10) Gao, B.; Liu, Z.-F. Ionization Induced Relaxation in Solvation Structure: A Comparison between $Na(H_2O)_n$ and $Na(NH_3)_n$. *J. Chem. Phys.* **2007**, *126*, 084501.

(11) Hashimoto, K.; Daigoku, K. Ground and Low-Lying Excited States of $Na(NH_3)_n$ and $Na(H_2O)_n$ Clusters: Formation and Localization of Solvated Electron. *Chem. Phys. Lett.* **2009**, *469*, 62-67.

(12) Uhlig, F.; Herbert, J. M.; Coons, M. P.; Jungwirth, P. Optical Spectroscopy of the Bulk and Interfacial Hydrated Electron from Ab Initio Calculations. *J. Phys. Chem. A.* **2014**, *118*, 7507-7515.

(13) Rolles, D.; Zhang, H.; Pešic, Z. D.; Bilodeau, R. C.; Wills, A.; Kukk, E.; Rude, B. S.; Ackerman, G. D.; Bozek, J. D.; Muiño, R. D.; *et al.* Size Effects in Angle-Resolved Photoelectron Spectroscopy of Free Rare-Gas Clusters. *Phys. Rev. A.* **2007**, *75*, 031201.

(14) Bartels, C.; Hock, C.; Huwer, J.; Kuhnen, R.; Schwöbel, J.; von Issendorff, B. Probing the Angular Momentum Character of the Valence Orbitals of Free Sodium Nanoclusters. *Science.* **2009**, *323*, 1323-1327.

(15) Sanov, A. Laboratory-Frame Photoelectron Angular Distributions in Anion Photodetachment: Insight into Electronic Structure and Intermolecular Interactions. *Annu. Rev. Phys. Chem.* **2014**, *65*, 341-363.

(16) Melko, J. J.; Castleman, A. W., Jr. Photoelectron Imaging of Small Aluminum Clusters: Quantifying s-p Hybridization. *Phys. Chem. Chem. Phys.* **2013**, *15*, 3173-3178.

(17) Khuseynov, D.; Blackstone, C. C.; Culberson, L. M.; Sanov, A. Photoelectron Angular Distributions for States of Any Mixed Character: An Experiment-Friendly Model for Atomic, Molecular, and Cluster Anions. *J. Chem. Phys.* **2014**, *141*, 124312.

(18) Kammrath, A.; Verlet, J. R. R.; Griffin, G. B.; Neumark, D. M. Photoelectron Imaging of Large Anionic Methanol Clusters: (MeOH)n(-) (n ~ 70-460). *J. Chem. Phys.* **2006**, *125*, 171102.

(19) Young, R. M.; Yandell, M. A.; Niemeyer, M.; Neumark, D. M. Photoelectron Imaging of Tetrahydrofuran Cluster Anions (THF)n(-) (1 ≤ n ≤ 100). *J. Chem. Phys.* **2010**, *133*, 154312.

(20) Signorell, R.; Yoder, B. L.; West, A. H. C.; Ferreiro, J. J.; Saak, C.-M. Angle-Resolved Valence Shell Photoelectron Spectroscopy of Neutral Nanosized Molecular Aggregates. *Chem. Sci.* **2014**, *5*, 1283-1295.

(21) West, A. H. C.; Yoder, B. L.; Signorell, R. Size-Dependent Velocity Map Photoelectron Imaging of Nanosized Ammonia Aerosol Particles. *J. Phys. Chem. A.* **2013**, *117*, 13326-13335.

(22) Yoder, B. L.; West, A. H. C.; Schläppi, B.; Chasovskikh, E.; Signorell, R. A Velocity Map Imaging Photoelectron Spectrometer for the Study of Ultrafine Aerosols with a Table-Top VUV Laser and Na-Doping for Particle Sizing Applied to Dimethyl Ether Condensation. *J. Chem. Phys.* **2013**, *138*, 044202.

(23) West, A. H. C.; Yoder, B. L.; Luckhaus, D.; Saak, C.-M.; Doppelbauer, M.; Signorell, R. Angle-Resolved Photoemission of Solvated Electrons in Sodium-Doped Clusters. *J. Phys. Chem. Lett.* **2015**, *6*, 1487-1492.

(24) Oana, C. M.; Krylov, A. I. Dyson Orbitals for Ionization from the Ground and Electronically Excited States within Equation-of-Motion Coupled-Cluster Formalism: Theory, Implementation, and Examples. *J. Chem. Phys.* **2007**, *127*, 234106.

(25) Oana, C. M.; Krylov, A. I. Cross Sections and Photoelectron Angular Distributions in Photodetachment from Negative Ions Using Equation-of-Motion Coupled-Cluster Dyson Orbitals. *J. Chem. Phys.* **2009**, *131*, 124114.

(26) Yamamoto, Y.; Suzuki, Y.-I.; Tomasello, G.; Horio, T.; Karashima, S.; Mitríc, R.; Suzuki, T. Time- and Angle-Resolved Photoemission Spectroscopy of Hydrated Electrons Near a Liquid Water Surface. *Phys. Rev. Lett.* **2014**, *112*, 187603.

(27) Peppernick, S. J.; Gunaratne, K. D. D.; Castleman, A. W., Jr. Superatom Spectroscopy and the Electronic State Correlation between Elements and Isoelectronic Molecular Counterparts. *Proc. Nat. Acad. Sci*. **2010**, *107*, 975-980.

(28) Humeniuk, A.; Wohlgemuth, M.; Suzuki, T.; Mitrić, R. Time-Resolved Photoelectron Imaging Spectra from Non-Adiabatic Molecular Dynamics Simulations. *J. Chem. Phys.* **2013**, *139*, 134104.

(29) Bartels, C. Angular Distributions of Photoelectrons from Cold, Size-Selected Sodium Cluster Anions [Ph.D. thesis]: Albert-Ludwigs-Universität; 2008.

(30) Yoder, B. L.; Litman, J. H.; Forysinski, P. W.; Corbett, J. L.; Signorell, R. Sizer for Neutral Weakly Bound Ultrafine Aerosol Particles Based on Sodium Doping and Mass Spectrometric Detection. *J. Phys. Chem. Lett.* **2011**, *2*, 2623-2628.

(31) Litman, J. H.; Yoder, B. L.; Schläppi, B.; Signorell, R. Sodium-Doping as a Reference to Study the Influence of Intracluster Chemistry on the Fragmentation of Weakly-Bound Clusters Upon Vacuum Ultraviolet Photoionization. *Phys. Chem. Chem. Phys.* **2013**, *15*, 940-949.

(32) Forysinski, P. W.; Zielke, P.; Luckhaus, D.; Corbett, J.; Signorell, R. Photoionization of Small Sodium-Doped Acetic Acid Clusters. *J. Chem. Phys.* **2011**, *134*, 094314.

(33) Eppink, A. T. J. B.; Parker, D. H. Velocity Map Imaging of Ions and Electrons Using Electrostatic Lenses: Application in Photoelectron and Photofragment Ion Imaging of Molecular Oxygen. *Rev. Sci. Instrum.* **1997**, *68*, 3477-3484.

(34) Chandler, D. W.; Houston, P. L. Two-Dimensional Imaging of State-Selected Photodissociation Products Detected by Multiphoton Ionization. *J. Chem. Phys.* **1987**, *87*, 1445-1447.

(35) Cooper, J.; Zare, R. N. Angular Distribution of Photoelectrons. *J. Chem. Phys.* **1968**, *48*, 942-943.

(36) Frisch, M. J.; Trucks, G. W.; Schlegel, H. B.; Scuseria, G. E.; Robb, M. A.; Cheeseman, J. R.; Scalmani, G.; Barone, V.; Mennucci, B.; Petersson, G. A.; *et al*. Gaussian 09. Wallingford, CT, USA: Gaussian, Inc.; 2009.

(37) Reed, A. E.; Weinstock, R. B.; Weinhold, F. Natural-Population Analysis. *J. Chem. Phys.* **1985**, *83*, 735-746.

Table of Contents Image